ejpmr, 2019,6(10), 503-513

SJIF Impact Factor 6.222

EUROPEAN JOURNAL OF PHARMACEUTICAL AND MEDICAL RESEARCH
www.ejpmr.com

Research Article
ISSN 2394-3211
EJPMR

A METHOD FOR AITIFACTS REMOVED FROM MRI OF BRAIN

Anubrta Das*, Soumen Halder, Arkadip Maitra, Shree Mitra and Raj Sen

India.

***Corresponding Author: Anubrta Das**
India.

Article Received on 08/08/2019 **Article Revised on 28/08/2019** **Article Accepted on 17/09/2019**

ABSTRACT

Improvement in detection and evaluation of brain abnormality and tissues detection is an important task in brain image analysis. Diagnosis quality of brain MR of brain images hampered due to the presence of artifacts. Small abnormalities detection hampered due to the presence of skull region of the brain.[1-4] Sometimes artifacts and skull have been treated as an abnormality in the automated system, and it hampers the intelligence system. Thus a computerized method requires pre-processed image as artifacts and skull removal. Pre-processing makes the image segmentation more accurate. In this paper, a pre-processing method for improvement of brain abnormality detection and diagnosis has been presented.

KEYWORDS: Brain Images, Segmentation, Artifacts and Pre-Processed Image.

INTRODUCTION

Automatic segmentation of brain tissues from MRI is a challenging process due to the variation in brain shapes and similarity of intensity values in the brain and non-brain tissues. Artifacts and undesired tissues (skull) as non-brain region affect the quality of processing and may lead to automatic diagnostic confusion.[8-12] It is done for the purpose of clearing away non-brain backgrounds and reducing unwanted information from the MR images. The majority of skull stripping treats the brain as a single connected region separated from non-brain tissues by a rim of CSF. In reality, even with high-resolution, T1 weighted MR images, thin connections between the brain and other cranial structures exist in the form of dura and connective tissue lining venous sinuses. In the present day artifacts in MRI are mainly letters that contain the patient's pieces of information and image modality.[13-20]

The proposed pre-processing is very simple technique using the combination of binarization, wavelet decomposition, and computational geometric as major intermediate steps. It tested with a large number of MR images and produced good results. In pre-processing, method artifacts removal is considered as mandatory, and skull removal is optional. Artifacts removal is required for every post-processing technique, and skull removal is required for some abnormality detection like edema, tumor, stroke lesions and hemorrhage lesions, but sometimes for a particular type of hemorrhage, we need the distance of abnormal region from the skull.[21-40]

Review Works

Some automated and semi-automated skull stripping algorithms are available in the literature. Skull removal using graph cuts[41-52] relies on graph theoretic image segmentation techniques to position cuts that serve to isolate and remove skull. Region growing based[53-81] method for coronal T1-weighted images plans to automatically detect two seed regions of the brain and non-brain by using the mask generated by mathematical morphological operations. Then the seed regions were expanded using 2D region growing algorithm. Another fully automatic brain extraction method[82] using diffusion, run length encoding, and region labeling was developed for skull removal in T2 weighted axial MR brain images. Clustering and 2D Region Growing method[83] for detecting the brain boundaries inside the skull was used to join the clusters and also remove the skull area. Authors are tested on four slices only thus method needed to improvement to process all the slices in the dataset. Robex method[84] for skull stripping by using a shape model trained on healthy brains to be relatively insensitive to lesions inside the brain. Their results showed this method was better than Brain Surface Extractor (BSE), hybrid watershed algorithm (HWA) and brain extraction tool (BET). They used T1 weight images taken from glioblastoma patients.

A method based[85] on histogram analysis and compared the segmentation accuracy between their proposed method and two widely used techniques, namely BSE and BET. Based on this factor, they reported that their proposed method outperforms these methods.

A deep convolutional learning[86] architecture is used to skull removal but not limited to non-enhanced T1 images. When trained appropriately, it handles an arbitrary number of modalities including contrast-enhanced scans. Its applicability to MRI data, comprising four channels: non-enhanced and contrast-enhanced T1w, T2w and FLAIR contrasts, is demonstrated on a challenging clinical data set containing brain tumors. A mathematical morphology method was implemented[87] for the pre-processing of MR brain images for the improved segmentation of brain tumor based on mathematical morphology operations. The first part of that paper[87] was an efficient method for the skull stripping of brain MR images based on mathematical morphology. In that paper, brain part was identified by the largest connected component in the image after binarization. The largest connected component is then dilated with a 3x3 square structuring element so as to preserve minute brain information in the output image. The holes in the resultant image were filled to make the brain a complete connected component. The resulting pixels are superimposed with the input image for getting the skull removed image. But the problem arises when skull and brain is connected then that method fails to identify the difference between brain and skull.

Most of these methods apply to specific a type of MR brain images and do not extract the brain completely in all the slices. Moreover, none of these presented methods give good performance when evaluated for large-scale data set. It is due to the complexity of the human brain, varying image contrast properties, image artifacts such as under-sampling, noise factor, variations in the image orientations and types.

Proposed Methodology

Artifacts removal is an essential task for normal and abnormality brain tissues identification. Skull elimination is another important step for abnormality segmentation. In the case of particular type of hemorrhage (e.g., chronic subdural hematoma) lesions segmentation skull information is required due to the distance measurement from the skull. Thus in pre-processing method skull removal is not mandatory for some few cases, it depends on applications. Figure 1 shows a flowchart of pre-processing of brain normal and abnormal tissue detection.

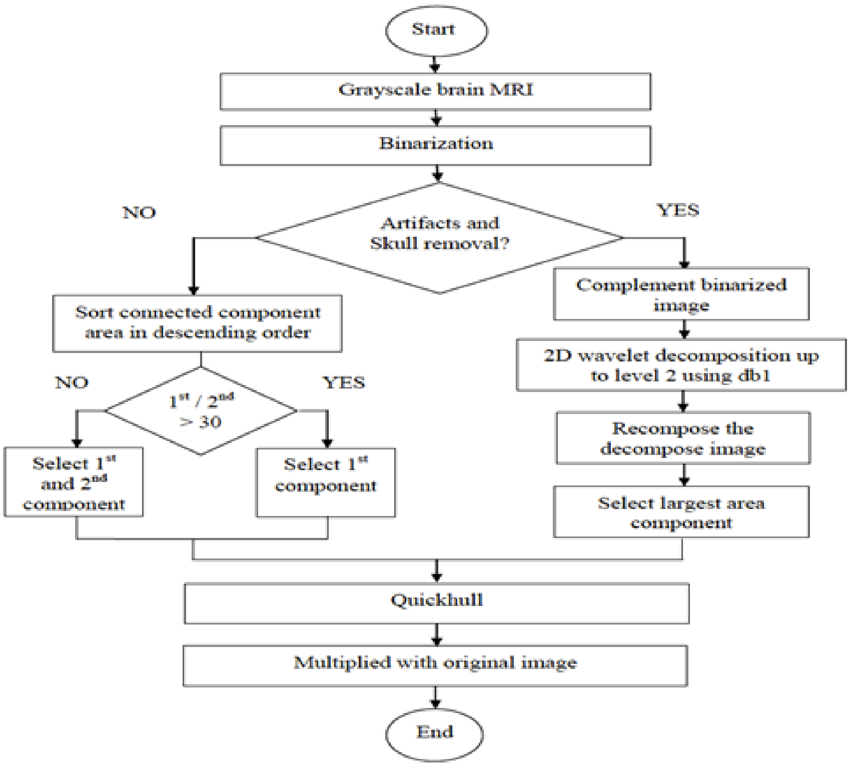

Figure 1: Flow diagram of pre-processing for brain abnormality and normal tissue detection.

A brain MRI first converted into a grayscale image, and then global threshold intensity has been calculated using standard deviation method. An image I[m,n] and h are the intensity of each pixel of the gray image. Thus the total intensity of the image is defined by.

$$T = \sum_{I} h[I] \quad (1)$$

The average intensity of the image is defined as the mean of the pixel intensity within that image, and the average intensity is defined as I_{avg} by.

$$I_{avg} = \frac{T}{m \times n} \quad (2)$$

The standard deviation S_d of the intensity within an image is the threshold value of the total image is defined by:

$$S_d = \sqrt{\frac{1}{(m \times n) - 1} \sum_{m,n \epsilon I} (I[m,n] - I_{avg})^2} \quad (3)$$

Here the threshold intensity S_d as of the entire image is unique. So, the binary image of an image I[m,n] is BI[m,n] is given by

$$BI[m,n] = 1 \qquad if I[m,n] \geq S_d$$

$$BI[m,n] = 0 \qquad if I[m,n] < S_d \quad (4)$$

Brain region, skull and many artifacts are converted into white pixels. This binarization step helps to perform connected generation in artifacts removal and wavelet decomposition in artifacts and skull removal. After binary image generation, we have an option of artifact and skull removal. Artifacts and skull removal is the one option and only artifacts removal as another option.

Artifacts Removal Intermediate Steps

Artifacts removal needs to perform following intermediate steps after performing above steps

(a) Compute the areas of each connected components, and descending order of areas are stored in an array. Connected component labeling works by scanning an image, pixel-by-pixel to identify connected pixel regions, i.e. regions of adjacent pixels which share the same set of intensity values V={1}. The connected components labeling operator scans the image by moving along a row until it comes to a point p (where p denotes the pixel to be labeled at any stage in the scanning process) for which V={1}. When this is true, it examines the four neighbors of p which have already been encountered in the scan (i.e. the neighbors (i) to the left of p, (ii) above it, and (iii and iv) the two upper diagonal terms). Based on this information, the labeling of p occurs as follows: i) If all four neighbors are 0, assign a new label to p, else ii) if only one neighbor has V={1}, assign its label to p, else iii) if more than one of the neighbors have V={1}, assign one of the labels to p and make a note of the equivalences.

After completing the scan, the equivalent label pairs are sorted into equivalence classes, and a unique label is assigned to each class. As a final step, a second scan is made through the image, during which each label is replaced by the label assigned to its equivalence classes.

(b) The connected component with the maximum area and second highest area are found out from descending order array. Then ratio between highest and second highest has been performed for the identification of head region (or brain without artifact). i) If the ratio is greater than high (e.g., >30), then keep only highest area and remove all other components. Ratio high (e.g., >30) signifies that the skull and brain are connected as one component, and thus it produces very high ratio between the brain and small artifact. That ratio in that case always produces high because artifacts are principally letters which have very less area individually. ii) If the ratio is less than 30 (high value is taken as 30), then select highest and second highest components and remove others components. If skull and main brain region are disconnected, then these two are treated as highest and second highest components. The ratio between the skull and main brain never exceeds 30.

Artifacts and Skull Removal Intermediate Steps

Artifacts and skull removal both need to perform following intermediate steps after performing above steps:

a. Complement the binarized image that helps for wavelet decomposition because we want to disconnect main brain region from skull where both are connected.

b. Two-dimensional wavelet decompositions are done using 'db1' wavelet up to level two. The connection between brain and skull region are removed when we recompose the image.

c. Re-composition of the image is done using the approximate coefficient of the previous step. Then resize the image of the previous step to the original size and re-complement of the image.

d. Select a largest connected area of from connected components and remove other components. This largest component is the brain without skull region in MRI.

After performing the artifacts or artifacts and skull removal steps, we use some common procedure. The binary image contains white pixels are losses some information in the border as well as inside the bounded area. To make it perfect as possible we perform quickhull[88] on white pixels. The quickhull algorithm uses less space than most of the randomized incremental algorithms and executes faster for inputs with non-extreme points. Computation time is less, and also, quickhull uses merged facets to guarantee that the output is clearly convex. Then that convex binarized image is multiplied with the original image to produce the final results.

Complexity

The time complexity regarding big-O for proposed pre-processing method has been described. Assuming input image has m number of row and n number of column and if some row = number of column = n then to compute the binarized image $O(n^2)$time required. Selection of maximum area require O(n) time, and convex hull computation takes O(n×n logn) time, and multiplication of each image pixel require $O(n^2)$ time. Thus the total time complexity: $T(n) = O(n^2) + O(n^2) + O(n\times n \log n) + O(n) \approx O(n^2 \log n)$.

RESULTS AND DISCUSSIONS

Proposed method gives suitable results for different MRI of brain images in artifacts removal as well as artifacts and skull removal. The results below have been tested visually and metrically. The procedure of proposed methods has been described above, and figures below show each functional step of the proposed methods. Figure 2 below shows the intermediary results of different intermediate steps of artifacts and skull removal methodology. Brain MRI image (a) is taken as input and converted it to a grayscale image for next step binarization. (b) Is the binarized output using the standard deviation based threshold intensity for the input image (a), Here maximum of brain region along with artifacts are very clearly visible in the binary image. This visibility of maximum brain tissues and artifacts are very useful for next steps. It is clear that the ratio of brain to artifact gives very high (i.e. above 30). The ratio between the skull and internal brain tissue will not exceed 30 in any case. So, depending on the ratio between highest to second highest component brain and skull has been selected. (c) Is the output after removing artifacts from the binary image but some loss of information may possible on the border of the image as well as inside of the image. To reduce the loss of information quickhull method has been used and the result is shown in (d). Pixel-wise multiplication has been performed between the input image (a) and quickhull image (d) and input image without artifacts is shown in (e). Reference image of without artifacts for input image has been shown in (f). Artifact removal by proposed method and reference image shows similar by visually which indicates good pre-processing. Different intermediate steps are required for artifacts and skull removal method. The complement of the binarized input image is shown (g) that help wavelet decomposition step. (h) Is output after applying wavelet decomposition using 'db1' wavelet up to level two. Using wavelet decomposition, we reduce the information within the image. If any connection exists in between skull and main brain region, then wavelet decomposition helps to disconnect between that connections. Due to the reduction of size in wavelet decomposition we recompose and resize the image to the initial size. The re-complemented and recomposed image has been shown in (i). Selection of largest area as the brain is easier as we disconnect the skull and main brain and largest area have been shown in (j). Some losses of information in (j) and to recover this loss quickhull method applied on (j). Applying quickhull generated correct result has been shown in (k). Then (l) is brain image without any artifacts and skull using the pixel-wise multiplication between the input image and convex image. Reference binary image of artifacts and skull removal for input (a) has been shown in (m). In visual prospect, both proposed method result and the reference image are almost similar.

(a) input brain MRI (b) binarized image (c) without artifacts

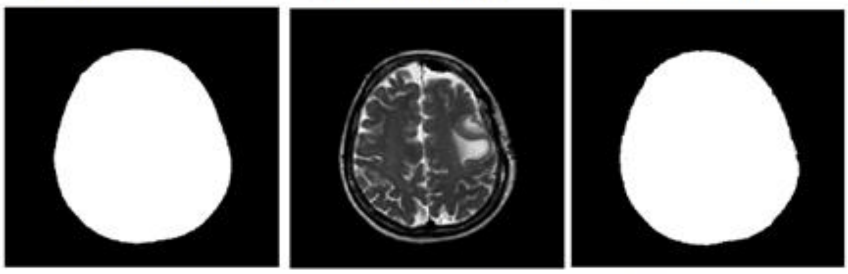

(d) applying quickhull (e) input image without artifacts (f) reference image without artifacts

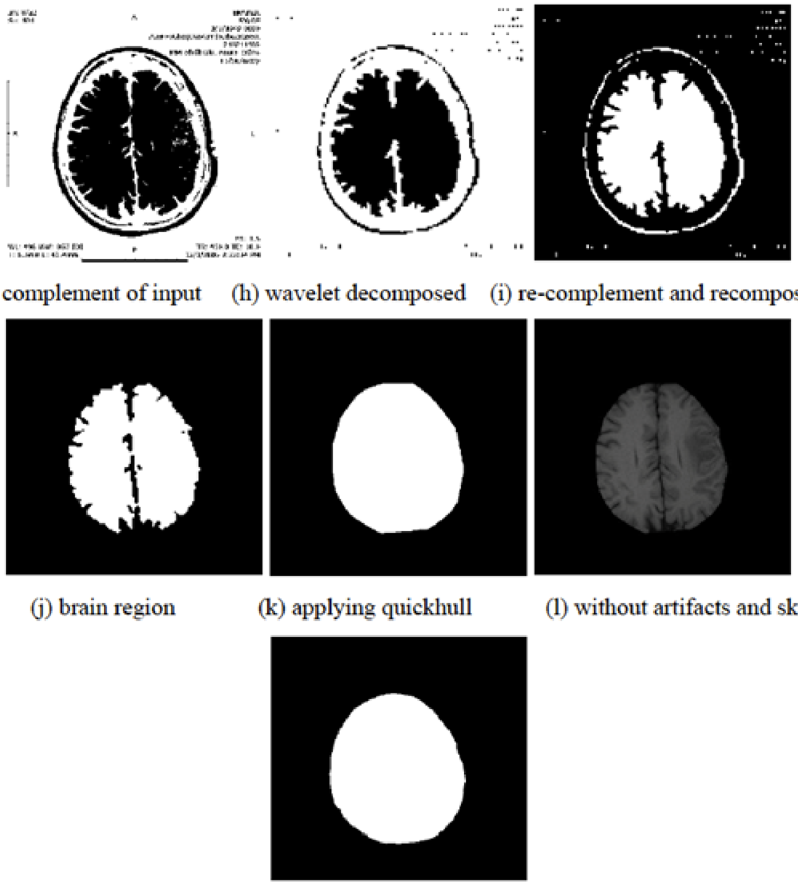

(g) complement of input (h) wavelet decomposed (i) re-complement and recomposed

(j) brain region (k) applying quickhull (l) without artifacts and skull

(m) reference image for removed artifacts and skull

Figure 2: Output of different intermediate steps of artifacts and skull removal methodology. (b) is the binarized output for input image (a), (c) is the output after artifacts removal, (d) is convex hull output on image (c), (e) is input image without artifacts, (f) is reference image of without artifacts for input image (a), (g) is complement of inputted binarized image (b), (h) is output after applying wavelet decomposition, (i) is re-complement and recomposed result on image (h), (j) is the output after removing skull region, (k) is result after applying convex hull to generate correct result, (l) is brain image without any artifacts and skull, and (m) is reference binary image of artifacts and skull removal for input (a).

Performance Measurement

Artifacts removal technique can remove the artifacts if any artifacts present in the brain MRI. Proposed method is tested on a large dataset and produce excellent results except for connected artifact with the original brain portion image. Proposed technique is very helpful in the sense of brain tissues detection. Artifacts and skull removal technique is also to remove skull and artifacts for different images. The correct elimination of skull and artifacts will reduce false detection in abnormal tissues detection. Measure the performance by visually may be biased. Thus some performance evaluation metrics are used to evaluate the error and accuracy with respect to the reference image.

The accuracy is used to evaluate the performance of the proposed methods are the Relative area Error (RAE or RE), Kappa Index (KI), Jacard Index (JI), Correct Detection Ratio (CDR) and False Detection Ratio (FDR). A critical problem faced in performance evaluation of artifacts and skull removal method is the lack of a gold standard. Here we use ground truth suggested by a radiologist for the comparison with the automated method and measures their performance with the help of RE, KI, JI, CDR, FDR.[89, 90] Let AS, and MS denote the area of the automatically segmented (AS) and manually segmented (MS) regions of the MR brain images. The Relative Error (RE) for the segmented region can be calculated as a division of the difference between ‘AS’ and ‘MS’ to ‘MS.' RE in percentage is given below.

$$RE = \frac{|AS - MS|}{MS} * 100\% \quad (5)$$

RE measure the relative area difference with respect to the manual ground truth segmented, in other words, we can say how much it differ from actual results. A method could be better when RE value is less, so the best method would be the minimum value of RE. The Kappa Index (KI) between two areas is calculated by the following equation (6).

$$KI(AS, MS) = \frac{(2|TP|)}{(|AS| + |MS|)} * 100\%$$

(6)

Here TP is the intersection of pixels between MS and AS, called true positive (TP), and it determines the correctness of method. KI determine correctness with respect to the automated and manual segmentation. KI is also represented as similarity index, which is sensitive to both differences in size and location. A method could be better when KI value is more, so the best method would be maximum value of KI. The Jaccard Index (JI) between two areas is represented as follow:

$$JI(AS, MS) = \frac{|TP|}{|TP + FN + FP|} * 100\%$$

(7)

Here false positive FP = AS – TP determine how much AS deviated from true positive and false negative FN = MS − TP determine how much MS deviated from true positive. This metric is further susceptible to variation since both denominator and numerator change with rising or falling overlap. Correct detection ratio (CDR) or sensitivity is defined by the following equation.

$$CDR = \frac{|AS \cap MS|}{MS} * 100\%$$

(8)

False detection ratio (FDR) is determine by

$$FDR = \frac{|AS - TP|}{MS} * 100\%$$

(9)

A Higher value of correct detection ratio and lower value of false detection ratio means the good results. A method could be better when JI and CDR value is more and less value of FDR so that the best method would be the maximum value of JI, and CDR and the minimum value of FDR. Different performance metric (AS, MS, RE, TP, FP, FN, KI, JI, CDR, FDR) has been shown in Table below for 0ten images[7] for evaluation errors and accuracy of our results. Proposed method has been tested on 450 images from different dataset.[5, 6, 7]

Segmented area of brain and brain without skull using proposed method with 341 × 341 image size has been shown in Table 1. Area of reference segmentation and the intersection between the reference and proposed method are also displayed in Table 1.Intersection pixels determines the exact number of pixels matches between automated segmented and manual (reference) segmented. The intersection nearer to the automated and manual segmentation indicates good segmentation and its intersection value has been shown in Table 1.

Table 1: Area of without artifacts and brain without skull using proposed and manual segmentation with their intersection.

Image sequence	Without Artifacts			Brain Without Skull		
	Automated	Manual	Intersection	Automated	Manual	Intersection
1	44246	45148	44232	30423	31062	30375
2	43672	44484	43649	28210	29125	28189
3	44135	44492	44125	30156	30483	30126
4	43581	44007	43389	29479	30282	29442
5	45278	45392	45198	30281	30933	30241
6	44288	45183	44206	29940	30426	29937
7	43218	44090	43183	28943	29471	28941
8	43826	44164	43820	29781	30282	29768
9	43002	44083	42960	29162	30001	29153
10	43539	44006	43502	29872	31206	29866

In medical imaging low error is required as much as possible because increased error reflects the wrong diagnosis. Removing artifacts and skull by keeping all necessary information (soft tissues of the brain) is the key goal of pre-processing. The relative area error (RE) and false detection ratio (FDR) for the brain with a skull (artifact removal) and without skull (artifacts and skull removal) are shown in Table 2.

Table 2: RE and FDR performance metric

Image sequence	RE		FDR	
	Without Artifacts	Brain Without Skull	Without Artifacts	Brain Without Skull
1	1.99	2.05	0.03	0.15
2	1.82	3.14	0.05	0.07
3	0.80	1.07	0.02	0.09
4	0.96	2.65	0.43	0.12
5	0.25	2.10	0.17	0.12
6	1.98	1.59	0.18	0.01
7	1.97	1.79	0.07	0.01
8	0.76	1.65	0.01	0.04
9	2.45	2.79	0.09	0.03
10	1.06	4.27	0.08	0.02

From the above table, all RE values in without artifacts are less than 3, and RE values in the brain without skull are less than 5. FDR values for both without artifacts and brain without skull are less than 1. RE less means that less over and under-segmentation, and FDR less means less false detection. In our preprocessing FDR and RE, both are very fewer values which indicate a good preprocessing. The column chart representation of RE and FDR values for ten images are shown in Figure 3 below.

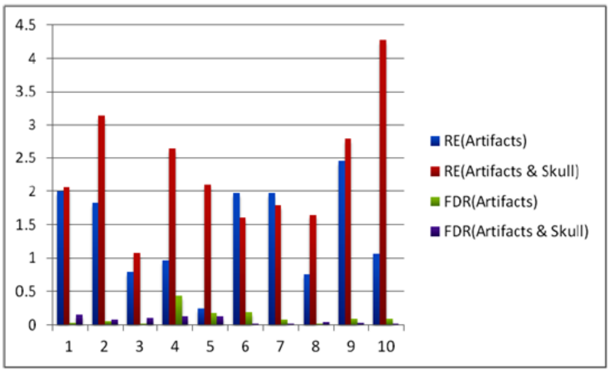

Figure 3: Column chart representation of RE and FDR metrics of preprocessing method.

From column chart, it is clear that maximum RE value is less than 3 and maximum FDR value is less than 2. Thus proposed pre-processing method is useful for brain abnormality detection as it generates a very low error.

The usefulness of pre-processing method also depends on correct segmentation or pre-processing. The values of different accuracy metrics KI, JI and CDR for pre-processing have been shown in Table 3 below.

Table 3: KI, JI, and CDR performance metric.

Image sequence	KI		JI		CDR	
	Without Artifacts	Brain Without Skull	Without Artifacts	Brain Without Skull	Without Artifacts	Brain Without Skull
1	98.96	98.80	97.94	97.64	97.97	97.79
2	99.03	98.33	98.07	96.72	98.12	96.78
3	99.57	99.36	99.15	98.73	99.18	98.82
4	99.08	98.53	98.16	97.11	98.60	97.22
5	99.68	98.80	99.39	97.64	99.57	97.76
6	98.82	99.18	97.66	98.38	97.83	98.39
7	98.92	99.09	97.86	98.19	97.94	98.20
8	99.60	99.12	99.21	98.26	99.22	98.30
9	98.66	98.55	97.36	97.14	97.45	97.17
10	99.38	97.80	98.77	95.69	98.85	95.71

Both without artifacts and brain without skull generates KI value greater than 98%. Thus this high KI indicates correctness with respect to the automated and manual segmentation. As KI is sensitive to both in size and location thus with respect to similarity measurement proposed pre-processing generates very good accuracy.

JI values for both methods are greater than 97% that indicates good accuracy. CDR values for both methods are greater than 97% that signifies pre-processing technique correctly segment the desired region of the brain.

The column chart representation of KI, JI and CDR values for ten images are shown in Figure 4.

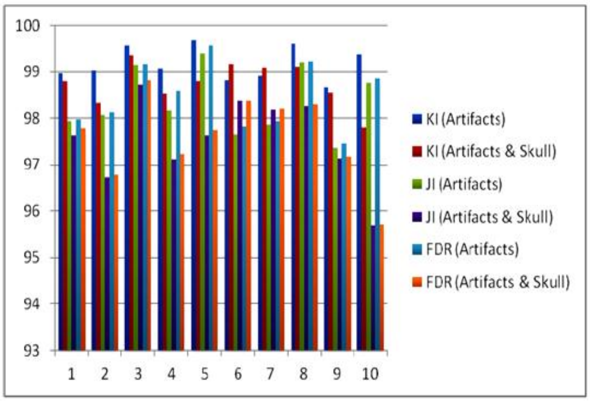

Figure 4: Column chart representation of KI, JI and CDR metrics of pre-processing method.

Proposed pre-processing technique generates very high accuracy which is clearly visible from column chart. High accuracy means correct identification, and it can be used as pre-processing. In another context, high accuracy increases the chances of good post-processing because good abnormality detection technique depends on good pre-processing.

The average value of performance evaluation metric RE, FDR, KI, JI, and CDR for ten images is shown in Table 4 below.

Table 4: Average value of error and accuracy metric.

Method name	RE	FDR	KI	JI	CDR
Artifacts	1.41	0.12	99.17	98.36	98.47
Artifacts and Skull	2.31	0.07	98.76	97.55	97.61

The average value of different error metrics is very less in both artifacts removal and artifacts and skull removal techniques. Average values of different accuracy metrics are also very high for both artifacts removal and artifacts and skull removal techniques. Thus a pre-processing with very high accuracy and very low error metric represents good pre-processing techniques.

CONCLUSIONS

In this paper, a fully automatic method for artifacts and skull removal of brain MR images using computational geometry, wavelet decomposition, and thresholding as intermediate steps has been described. Thresholding using standard deviation method is the key intermediate step to correct pre-processing of MR images. The proposed pre-processing method has high accuracy and low error rate for different MR images. This pre-processing is used to reduce the false detection. Thus it increases the diagnosis quality of disease from MRI of the brain by a computer system. Thus reprocessing with low error and high accuracy does not hamper the post-processing of intelligence system. The proposed method is very useful and important pre-processing for correct automated detection of brain abnormalities. This pre-processing method is used in abnormalities detection, segmentation and classification and tissues identification in this research.

REFERENCES

1. IARC: GLOBOCAN 2012. Estimated Cancer Incidence, Mortality and Prevalence Worldwide [Online: http://globocan.iarc.fr/Default.aspx].
2. The Multiple Sclerosis International Federation (MSIF). [2016 Online: http://www.msif.org].
3. Ei Sayed Ahmed EI Dahshan, Tamer Hosny and Abdel Badeeh M. Salem, “Hybrid intelligent techniques for MRI brain images classification,” Digital Signal Processing, Elsevier, 2010; 20(2): 433-441.
4. P. E. Ricci, and D. H. Dungan, “Imaging of low- and intermediate-grade gliomas,” Seminars in Radiation Oncoloy, 2001; 11(2): 103-112.
5. Whole Brain Atlas: MR brain image [online (2013): http://www.med.harvad.edu/AANLIB/home.html]
6. Brain Web: Simulated Brain MR brain image dataset [online (2013): http://brainweb.bic.mni.mcgill.ca/brainweb/]
7. The EASI MRI Home: MR brain image [online (2013): http://www.easidemographics.com/cgi-bin/dbmri.asp]
8. About brain tumors: a primer for patients and caregivers, Amirican brain tumor association, [Online:http://www.abta.org/secure/about-brain-tumors-a-primer.pdf] Copyright © 2015 ABTA, 2015; 1-84.
9. O Maier, C Schröder, ND Forkert, T Martinetz, H Handels, “Classifiers for Ischemic Stroke Lesion Segmentation: A Comparison Study,” PLoS ONE, 2015; 10(12): 1-16.
10. Fazeel M. Siddiqui, Simon V. Bekker, and Adnan I. Qureshi, "Neuroimaging of Hemorrhage and Vascular Defects," Neurotherapeutics: The Journal of the American Society for Experimental Neurotherapeutics, 2011; 8(1): 28-38.
11. Silvia Messina, Francesco Patti, "Gray Matters in Multiple Sclerosis: Cognitive Impairment and Structural MRI," Multiple Sclerosis International, Hindawi Publishing Corporation, volume 2014, Issue January, Article ID 609694, 2014; 1-9.
12. Mehmet Sezgin, Bu¨lent Sankur, "Survey over image thresholding techniques and quantitative performance evaluation," Journal of Electronic Imaging, 2004; 13(1): 146–165.
13. N. Otsu, “A Threshold Selection Method from Gray Level Histograms”, IEEE Trans. on System, Man and Cybernetics SMC, 1979; 9(1): 62–66.
14. Ankit Vidyarthi, Namita Mittal, "A Hybrid Model for Extraction of Brain Tumor in MR Images,"

International Conference on Signal Processing and Communication (ICSC), IEEE, 2014; 202-206.
15. Arashdeep Kaur, "An Automatic Brain Tumor Extraction System using Different Segmentation Methods," International Conference on Communication, Information & Computing Technology, IEEE, 2016; 178-191.
16. J. Bernsen, "Dynamic thresholding of gray level images," In: ICPR'86: Proceedings of the International Conference on Pattern Recognition, 1986; 1251–1255.
17. W. Niblack, "An Introduction to Digital Image Processing," Prentice Hall, Eaglewood, Cliffs, 1986; 115–116.
18. J. Sauvola, M. Pietikainen, "Adaptive document image binarization," Pattern Recognition, 2000; 33(2): 225–236.
19. J. N. Kapur, P. K. Sahoo, A. K. C. Wong "A New Method for Gray-Level Picture Thresholding Using the Entropy of the Histogram," Computer Vision, Graphics, And Image Processing, 1985; 29(3): 273-285.
20. R. C. Gonzalez, R. E. Woods, "Digital Image Processing," Second Edition, Prentice Hall, New Jersey, 2002.
21. Ursula Perez-Ramirez, Estanislao Arana, David Moratal, "Brain Metastases Detection on MR by Means of Three-Dimensional Tumor-Appearance Template Matching," International Society for Magnetic Resonance in Medicine, 2016; 44(3): 642-651.
22. Abd El Kader Isselmou, Shuai Zhang, Guizhi Xu, "A Novel Approach for Brain Tumor Detection Using MRI Images," J. Biomedical Science and Engineering, volume 9, Issue September, 2016; 44-52.
23. Nuno Vieira Lopes, Pedro A. Mogadouro do Couto, Humberto Bustince, and Pedro Melo-Pinto, "Automatic histogram threshold using fuzzy measures," IEEE Transactions on Image Processing, 2010; 19(1): 199-204.
24. Noor Elaiza Abdul Khalid, Shafaf Ibrahim, Mazani, Umi Kalthum Ngah "Seed-Based Region Growing Study for Brain Abnormalities Segmentation," 2010 International Symposium in Information Technology (ITSim), IEEE, 2010; 556-560.
25. Badri Narayan Subudhi, Veerakumar Thangaraj, Esakkirajan Sankaralingam, Ashish Ghosh, "Tumor or abnormality identification from magnetic resonance images using statistical region fusion based segmentation," Magnetic Resonance Imaging, ELSEVIER, 2016; 34(9): 1292–1304.
26. A. Javadpour, A. Mohammadi, "Improving Brain Magnetic Resonance Image (MRI) Segmentation via a Novel Algorithm based on Genetic and Regional Growth," J Biomed Phys Eng, 2016; 6(2): 95-108.
27. Padraig Cunningham, Sarah Jane Delany "k-Nearest Neighbour Classifiers", Technical Report UCD-CSI-2007-4, March 27, 2007.
28. Mohammed Sabbih Hamoud Al-Tamimi, Ghazali Sulong, "Tumor Brain Detection Through MR Images: A Review Of Literature, " Journal of Theoretical and Applied Information Technology, 2014; 62(2): 387-403.
29. T. Kalaiselvi , K. Somasundaram, M. Rajeswari, "Fast Brain Abnormality Detection Method for Magnetic Resonance Images (MRI) of Human Head Scans Using K-Means Clustering Technique," Proceedings of the Fourth International Conference on Signal and Image Processing 2012, Volume 221 of the series Lecture Notes in Electrical Engineering, 2012; 225-234.
30. Jason J. Corso, Eitan Sharon, ShishirDube, Suzie El-Saden, UshaSinha, and Alan Yuille, "Efficient Multilevel Brain Tumor Segmentation with Integrated Bayesian Model Classification, " IEEE Transactions on medical imaging, 2008; 27(5): 629–640.
31. Evangelia Zacharaki and Anastasios Bezerianos, "Abnormality Segmentation in Brain Images Via Distributed Estimation," IEEE Transactions On Information Technology In Biomedicine, 2012; 16(3): 330-338.
32. Eloy Roura, Nicolae Sarbu, Arnau Oliver, Sergi Valverde, Sandra González-Villà, Ricard Cervera, Núria Bargall,and Xavier Lladó, "Automated Detection of Lupus White Matter Lesions in MRI," Front. Neuroinform, volume 10, Issue August, 2016; 1-33.
33. Yuri Boykov, Olga Veksler, RaminZabih, "Markov Random Fields with Efficient Approximations," Proceedings of IEEE conference on Computer Vision and Pattern Recognition (CVPR), IEEE Computer Society, 1998; 648-655.
34. Qolamreza R. Razlighi, Aleksey Orekhov, Andrew Laine,and Yaakov Stern, "Causal Markov Random Field For Brain MR Image Segmentation," Conf Proc IEEE Eng Med Biol Soc, 2012; 3203–3206.
35. Hayder Saad Abdulbaqi, Mohd Zubir Mat Jafria, Kussay N. Mutter, Ahmad Fairuz Omar, "Segmentation and Estimation of Brain Tumor Volume in Magnetic Resonance Images Based on T2-Weighted using Hidden Markov Random Field Algorithm," Journal of Telecommunication, Electronic and Computer Engineering, 2016; 8(3): 1-5.
36. S. Ruan, S Lebonvallet, A. Merabet, J. Constans, "Tumor segmentation from a multispectral MRI images by using support vector machine classification," In ISBI, pages 1236–1239, Washington, USA, 2007.
37. R. Rajesh Sharma and P. Marikkannu, "Hybrid RGSA and Support Vector Machine Framework for Three-Dimensional Magnetic Resonance Brain Tumor Classification," The Scientific World Journal, volume 2015, Article ID 184350, 14 pages, 2015.
38. Marco Alfonse and Abdel-Badeeh M. Salem, "An Automatic Classification of Brain Tumors through

MRI Using Support Vector Machine," Egyptian Computer Science Journal, September 2016; 40(03): 11-21.
39. D. Zhang, S. Chen, "A novel kernelized fuzzy c-means algorithm with application in medical image segmentation," Artificial Intelligence in Medicine, ELSEVIER, September 2004; 32(1): 37–50.
40. Mutasem Alsmadi, "MRI Brain Segmentation Using a Hybrid Artificial Bee Colony Algorithm with Fuzzy-C Mean Algorithm," Journal of Applied Sciences, 2015; 15(1): 100-109.
41. Eman Abdel-Maksouda, Mohammed Elmogy, Rashid Al-Awadic, "Brain tumor segmentation based on a hybrid clustering technique," Egyptian Informatics Journal, 2015; 16(1): 71–81.
42. Parveen, Amritpal Singh, "Detection of Brain Tumor in MRI Images, Using Fuzzy C-Means Segmented Images and Artificial Neural Network," Proceedings of the International Conference on Recent Cognizance in Wireless Communication & Image Processing, 2016; 123-131.
43. M. C. Jobin Christ, R. M. S. Parvathi, "Segmentation of Medical Image using K-Means Clustering and Marker Controlled Watershed Algorithm", European Journal of Scientific Research, 2012; 71(2): 190-194.
44. A. Naveen, T. Velmurugan, "Identification of Calcification in MRI Brain Images by k-Means Algorithm," Indian Journal of Science and Technology, November 2015; 8(29): 1-7.
45. Jianwei Liu, Lei Guo, "An Improved K-means Algorithm for Brain MRI Image Segmentation," ICMRA 2015, Atlantis Press, 2015; 1087-1090.
46. J. Rexilius, K. Hahn, J. Klein, M. Lentschig, H. Peitgen, "Multispectral brain tumor segmentation based on histogram model adaptation," In SPIE, 2007; 6514-65140V, San Diego, USA.
47. Jin Liu, Min Li, Jianxin Wang, Fangxiang Wu, Tianming Liu, and Yi Pan, "A Survey of MRI-Based Brain Tumor Segmentation Methods," Tsinghua Science and Technology, 2014; 19(6): 578-595.
48. J. Dolz, L. Massoptier, M. Vermandel, "Segmentation algorithms of subcortical brain structures on MRI for radiotherapy and radiosurgery: A survey," IRBM, 2015; 36(4): 200-212.
49. Lin Li, Mary Cazzell, Olajide Babawale, Hanli Liu, "Automated voxel classification used with atlas-guided diffuse optical tomography for assessment of functional brain networks in young and older adults," Neurophoton, SPIE, 2016; 3(4): 1-8.
50. Umer Javed, Muhammad M. Riaz, Abdul Ghafoor, and Tanveer A. Cheema1, "MRI Brain Classification Using Texture Features, Fuzzy Weighting And Support Vector Machine," Progress In Electromagnetics Research B, 2013; 53: 73–88.
51. M. Syed Reza, Atiq Islam, M. Khan, "Texture Estimation for Abnormal Tissue Segmentation in Brain MRI," The Fractal Geometry of the Brain Part of the series Springer Series in Computational Neuroscience, 2016; 333-349.
52. Deepa Subramaniam Nachimuthu and Arunadevi Baladhandapani, "Multidimensional Texture Characterization: On Analysis for Brain Tumor Tissues Using MRS and MRI," J Digit Imaging, 2014; 27(4): 496–506.
53. A. Shenbagarajan, V. Ramalingam, C. Balasubramanian and S. Palanivel, "Tumor Diagnosis in MRI Brain Image using ACM Segmentation and ANN-LM Classification Techniques," Indian Journal of Science and Technology, 2016; 9(1): 1-12.
54. P. Balasubramanian, S. ManjuAffiliated, "An Advanced Magnetic Resonance Imaging Technique for the Detection of Abnormal Changes Using Artificial Neural Network," Artificial Intelligence and Evolutionary Computations in Engineering Systems, 394 of the series Advances in Intelligent Systems and Computing, 2016; 1085-1091.
55. Kamil Dimililer, Ahmet İlhan, "Effect of Image Enhancement on MRI Brain Images with Neural Networks," Procedia Computer Science, August 2016; 102: 39-44.
56. Tang X, Crocetti D, Kutten K, et al. "Segmentation of brain magnetic resonance images based on multi-atlas likelihood fusion: testing using data with a broad range of anatomical and photometric profiles," Frontiers in Neuroscience, 2015; 9(61): 1-13.
57. Chakravarty, M. Mallar et al. "Performing Label-Fusion-Based Segmentation Using Multiple Automatically Generated Templates," Human brain mapping, PMC. Web, 2016; 34(10): 2635–2654.
58. C. Li, C.-Y. Kao, G. J. C., and Z. Ding, "Minimization of Region-Scalable Fitting Energy for Image Segmentation," IEEE Transactions on Image Processing, 2008; 17(10): 1940-1949.
59. Hyun Joon An, Seongho Seo et. al., "MRI-Based Attenuation Correction for PET/MRI Using Multiphase Level-Set Method," J Nucl Med, 2016; 57(4): 587–593.
60. C. M. Naveen Kumar , B. Ramesh, J. Chandrika, "Design and Implementation of an Efficient Level Set Segmentation and Classification for Brain MR Images," Artificial Intelligence and Evolutionary Computations in Engineering Systems 394 of the series Advances in Intelligent Systems and Computing, 2016; 559-568.
61. Malladi R, Sethia JA, Vemuri BC. "Shape modeling with front propagation: a level set approach", IEEE Trans PAMI, 1995; 17(2): 158–175.
62. L. Vincent, P. Soille," Watersheds in digital spaces: an efficient algorithm based on immersion simulation", IEEE Trans Pattern Anal Mach Intell, 1991; 13(6): 583–598.
63. Wei-Guang Teng, Ping-Lin Chang, "Denitrifying Regions of Interest in Medical Images Using Self-Organizing Maps," Journal of Medical Systems, 2012; 36(5): 2761–2768.

64. Praveen Kumar Prajapati, Manish Dixit, "Un-Supervised MRI Segmentation using Self Organised Maps," 2015 International Conference on Computational Intelligence and Communication Networks, IEEE, 2015; 471-474.
65. Y. Pavan Kumar Reddy and G. Kesavan, "Tumor Identification Using Self Organizing MAP and BFR Algorithm," Middle-East Journal of Scientific Research, 2016; 24(6): 2110-2115.
66. T.Logeswari, M.Karnan, "Hybrid Self Organizing Map for Improved Implementation of Brain MRI Segmentation, "2010 International Conference on Signal Acquisition and Processing, IEEE computer society, 2010; 248-252.
67. Toshimitsu Otani, Kazuhito Sato, Hirokazu Madokoro, Atsushi Inugami, "Segmentation of head MR images using hybrid neural networks of unsupervised learning" The 2010 International Joint Conference onNeural Networks (IJCNN), IEEE, 2010; 1-7.
68. Y. Zhao, Y. Liu, X. Wu, S. Harding SP, Y. Zheng, "Correction: Retinal Vessel Segmentation: An Efficient Graph Cut Approach with Retinex and Local Phase," PLOS ONE, 2015; 10(4).
69. Benjamin Puccio, James P. Pooley, John S. Pellman, Elise C. Taverna and R. Cameron Craddock, "The preprocessed connectomes project repository of manually corrected skull-stripped T1-weighted anatomical MRI data," Giga Science, 2016; 45(5): 1-7.
70. Atiq Islama , M. Iftekharuddin, Robert J. Ogg, Fred H. Laningham, Bhuvaneswari Sivakumar, "Multifractal modeling, segmentation, prediction and statistical validation of posterior fossa tumors", Medical Imaging 2008: Computer-Aided Diagnosis, Proc. of SPIE 6915, 2008.
71. Guihu Zhao, Kristina Denisova, Pejman Sehatpour, Jun Long, Weihua Gui, Jianping Qiao, Daniel C. Javitt, and Zhishun Wang," Fractal Dimension Analysis of Subcortical Gray Matter Structures in Schizophrenia," PLoS One, 2016; 11(10): 1-23.
72. S Luo, R. Li, S. Ourselin, "A new deformable model using dynamic gradient vector flow and adaptive balloon forces," APRS Workshop on Digital Image Computing, Australia, http://citeseerx.ist.psu.edu/viewdoc/download?doi=10.1.1.3.1500&rep=rep1&type=pdf, 2003.
73. D. Jayadevappa, S Srinivas Kumar, D. S. Murty, "Medical image segmentation Algorithms using Deformable Models: A review", IETE technical review, 2014; 28(3): 248-255.
74. Ali M. Hasan, Farid Meziane, Rob Aspin and Hamid A. Jalab, "Segmentation of Brain Tumors in MRI Images Using Three-Dimensional Active Contour without Edge," Symmetry MDPI, 2016; 8(11): 1-32.
75. Hayder Saad Abdulbaqi, Mohd Zubir Mat, Ahmad Fairuz Omar, Iskandar Shahrim Bin Mustafa, Loay Kadom Abood, "Detecting brain tumor in Magnetic Resonance Images using Hidden Markov Random Fields and Threshold techniques View Document," 2014 IEEE Student Conference on Research and Development (SCOReD), IEEE, 2014; 1-5.
76. Chen, Ying, and Tuan D Pham. "Development of a Brain MRI-Based Hidden Markov Model for Dementia Recognition," BioMedical Engineering OnLine, PMC. Web, 2016; 12(1): 1-12.
77. Minakshi Sharma, Sourabh Mukharjee, "Brain Tumor Segmentation Using Genetic Algorithm and Artificial Neural Network Fuzzy Inference System (ANFIS)," Advances in Computing and Information Technology, AISC, Springer, 2013; 177: 329-339.
78. A. R. Kavitha, C. Chellamuthu, "Brain tumour segmentation from MRI image using genetic algorithm with fuzzy initialisation and seeded modified region growing (GFSMRG) method," The Imaging Science Journal, 2016; 64(5): 285-297.
79. G. Rajesh Chandra, Kolasani Ramchand H. Rao, "Tumor Detection In Brain Using Genetic Algorithm," Procedia Computer Science, 2016; 79: 449-457.
80. A.S. Suresh, W. Zheng, W.L.C. Michael, V. Zagorodnon, "Skull Stripping using Graph Cuts," Neuroimage, 2010; 49(1): 225-239.